Journal of Alloys and Compounds 642 (2015) 15–21

Contents lists available at ScienceDirect

Journal of Alloys and Compounds

journal homepage: www.elsevier.com/locate/jalcom

Tunable dielectric constant with transition metals doping in $Zn_{1-x}(MnTM)_xO$ (TM = Co, Fe) nanocrystals

Swati Singh, P. Dey, J.N. Roy, S.K. Mandal *

Department of Physics, National Institute of Technology Agartala, Agartala, Tripura 799046, India

ARTICLE INFO

Article history:
Received 3 March 2015
Received in revised form 27 March 2015
Accepted 9 April 2015
Available online 21 April 2015

Keywords:
Nanoparticles
Dielectric
Semiconductors

ABSTRACT

We have presented dielectric studies on $Zn_{1-x}Mn_{x/2}Fe_{x/2}O$ and $Zn_{1-x}Mn_{x/2}Co_{x/2}O$ (x = doping level) semiconducting nanoparticles (~2–40 nm). Structural analyses show the formation of single phase nanoparticles. Dielectric constant (ε) is found to exhibit sensitive modulation, both with the variation of doping element (Fe and Co) and doping level (x) in ZnMnO matrix and also with frequency (f). Enhancement of ε is found to be ~1500 times for $Zn_{0.9}Mn_{0.05}Fe_{0.05}O$ and ~2 times for $Zn_{0.9}Mn_{0.05}Co_{0.05}O$ from that of $Zn_{0.9}Mn_{0.1}O$ nanoparticles at low frequency region. The enhancement in ε can be explained on the basis of dielectric polarization, caused by the presence of different abundance of higher oxidation states of Fe and Co ions in ZnMnFeO and ZnMnCoO samples. From our observation one can choose the suitable doping element, along with suitable dopant concentration to achieve the desired higher value of ε in transition metal doped ZnMnO nanoparticles at room temperature. We have also estimated semiconducting band gap of those nanoparticles using recorded absorbance spectra.

1. Introduction

Nanomaterials have fascinated researchers in recent years because these materials exhibit unusual physical properties, such as optical, electrical and magnetic properties, as compared to their bulk counterpart. One of them is nanostructured zinc oxide (ZnO), which is well known for its wide band gap of 3.34 eV and large exciton binding energy of 60 meV. In general, ZnO is a material of huge application in spintronics [1], sensors [2], fabric industries [3] etc. Recently, there is an increasing research interest in semiconductor nanocrystal considering the issue of size miniaturization in semiconductor industry and surface state on nanometer scale [4]. In this attempted, a huge amount of research effort has been directed toward nanostructured ZnO. Also high dielectric constant (ε) material also has its wide application in microelectronic devices [5] and memory based devices [6]. In this direction the study of dielectric property of ZnO is gaining attention as well due to its optical transparency and mechanical flexibility [7] and is used as dielectric layer in device fabrication such as memory or micro-laser [8]. Omar reported the temperature and frequency dependent ε of bulk ZnO [9]. Ghosh et al. reported the high frequency ε and static ε of ZnO nanoparticle exhibiting a strong dependence on doping element, like Ni [10]. Recently, a review has been done on control doping and unintentional formation of impurities during growth of ZnO nanoparticles that advances in device processing techniques [11]. Yang et al. reported that ε of ZnO nanowire depends on diameter of the nanowire, i.e., as the diameter of the ZnO nanowire decreases, ε also decreases [12]. In general, Some of the research groups studied ε of nanoparticles, e.g., fine grained powder of diamond, silicon, LiF, NaCl and have shown a strong dependence of ε on crystal grain size [13]. Furthermore, in case of doped sample ε depends on composition of doping element [14].

Recently, a large number of studies on different kind of transition metal (TM) doped ZnO nanoparticles have been carried out by different research groups [15]. Many researchers are fascinated toward diluted magnetic semiconductor (DMS), which is promising for application in spintronic devices. Moreover, some research groups have shown that doping of TM into ZnO matrix lead to fine tuning of band gap. This feature can find application in *ultra violet* (UV) detectors and light emitters [16]. In our previous papers, we have shown room temperature antiferromagnetic (AFM)-like ground state for Co doped ZnO [17], ferromagnetic (FM)-like behavior for Fe doped ZnO [18] and mixed ferrimagnetic-FM like behavior for co – Fe and Co doped ZnO [19]. Recently, we have found enhancement in ε at room temperature for Fe-doped, Co-doped and Fe–Co co-doped ZnO nanoparticles, as well [20]. In this present work, we have focussed on the dielectric study of co-doped $Zn_{1-x}Mn_{x/2}TM_{x/2}O$ (Co, Fe) nanoparticles, where we have carried out the study by keeping Mn doping fixed and tuning TM(= Co,

---

* Corresponding author. Tel.: +91 3812348530.
E-mail address: saniitkgp2007@gmail.com (S.K. Mandal).

http://dx.doi.org/10.1016/j.jallcom.2015.04.092
0925-8388/© 2015 Elsevier B.V. All rights reserved.

Fe) doping. In this attempt, detailed dielectric studies have been carried out on Fe and Co doped $Zn_{1-x}Mn_{x/2}TM_{x/2}O$ nanoparticles with varying dopant concentration (x) at room temperature. Here we have shown how ε *strongly and sensitively* depends on both doping level and choice of the doping element as well. We have also reported a large enhancement of ε for both Fe and Co doped $Zn_{1-x}Mn_{x/2}TM_{x/2}O$ nanoparticles, as compared to ZnMnO nanoparticles at room temperature. Enhancement of ε for Fe doped sample is found to be larger as compared to Co doped ZnMnO matrix. Particle sizes of the samples are found to be in nanometric region, which has been confirmed from structural analysis. Semiconducting band gap of those samples have been estimated from absorbance spectra at room temperature.

2. Experimental details

$Zn_{1-x}Mn_xO$, $Zn_{1-x}Mn_{x/2}Co_{x/2}O$ and $Zn_{1-x}Mn_{x/2}Fe_{x/2}O$ nanoparticles were prepared by low temperature chemical "pyrophoric reaction process" [17,18,21–23]. The required chemicals were $Zn(NO_3)_2{\cdot}6H_2O$ for Zn, $Co(NO_3)_2{\cdot}6H_2O$ for Co, $Fe(NO_3)_3{\cdot}9H_2O$ for Fe, $C_4H_6MnO_4{\cdot}4H_2O$ for Mn, triethanolamine (TEA) and HNO_3. The requisite amount of $Zn(NO_3)_2{\cdot}6H_2O$, $C_4H_6MnO_4{\cdot}4H_2O$, $Fe(NO_3)_3{\cdot}9H_2O$, and $Co(NO_3)_2{\cdot}6H_2O$, depending on the required doping concentration (x), were mixed with distilled water. All the nitrates were soluble in distilled water. Then the solution was heated at ~190 °C with continuous stirring. After some time, TEA was added maintaining 1:4 ratio with metal ions and TEA, with metal ions were precipitated in the solution. At the same temperature HNO_3 was added to dissolve the precipitation and then the clear solution was evaporated with constant stirring. After complete dehydration, the nitrate themselves were decomposed with the evolution of brown fumes of NO_2 leaving behind a voluminous, organic based, brownish black, fluffy powder, i.e., precursor powder. The precursor powder, after grinding, was calcined at temperatures of 300–500 °C in air for 4 h to get nanocrystalline powders. We made circular pellets from calcined nano powders and have sintered them for 30–45 min. The sintering temperatures were same as that of calcination temperatures of the respective nano powders. These pellets have been used for transport, magnetic and optical studies. Details of the low temperature chemical reaction were according to

$$\begin{aligned}
&(1-x)\,Zn(NO_3)_2 + (x/2)\,C_4H_6MnO_4\cdot 4H_2O + (x/2)\,Fe(NO_3)_3/(x/2)\,Co(NO_3)_2\\
&\quad + N(CH_2CH_2OH)_3\\
&\quad \rightarrow [Zn - N(CH_2CH_2OH)_3]^{2+} + [Mn - N(CH_2CH_2OH)_3]^{2+}\\
&\qquad + [Fe - N(CH_2CH_2OH)_3]^{2+}/[Co - N(CH_2CH_2OH)_3]^{2+} + NO_3^-\\
&\quad \rightarrow \text{Oxidization in air}\\
&\quad \rightarrow Zn_{1-x}Mn_xO\ Zn_{1-x}Mn_{x/2}Fe_{x/2}O/Zn_{1-x}Mn_{x/2}Fe_{x/2}O\ (\text{nanosized}) + CO_2 + NO_2\\
&\qquad + N_2 + H_2O.
\end{aligned}$$

Structural characterisations have been done by X-ray diffraction technique (XRD) (Philips, PW-1729) with monochromatic Cu Kα radiation, Transmission electron microscopy (TEM) (JEOL, JEM-2100, 200 kV) and high resolution field emission scanning electron microscopy (FE-SEM) (Carl Zeiss, SUPPRA TM^{40}). Energy dispersive X-ray analysis (EDAX) has been done using Carl Zeiss, SUPPRA TM^{40}. Thermogravimetric analysis (TG) and differential thermal analysis (DTA) have been done in presence of air atmosphere with alumina crucible and with ramping rate of 10 °C/min, using Perkin Elmer Phyris Diamond TG-DTA. Detailed dielectric studies have been carried out using Agilent impedance analyser (4294 A) along with a homemade proportional–integral–derivative (PID) controlled furnace (300–600 K). We have used high purity and highly conducting silver paste for the preparation of electrodes on our pelletized samples. The copper wire has been used as the connecting electrical leads for electrical connection of those samples to the four probe cable of impedance analyser. Then the sample was kept on a flat surface of an asbestos sheet and has been placed inside the furnace (at middle position). For optical characterization of semiconducting nanoparticles, room temperature absorbance spectra were recorded using UV – visible spectrophotometer (Micro pack, DH-2000).

3. Results and discussions

3.1. Structural characterizations

Structural characterisations have been done by XRD, FE-SEM, TEM and TG-DTA. XRD patterns of $Zn_{0.8}Mn_{0.1}Fe_{0.1}O$ and $Zn_{0.9}Mn_{0.05}Fe_{0.05}O$ samples, calcined at temperatures of 300, 400 and 500 °C, are shown in Fig. 1(a) and (b), respectively. Similar, XRD patterns of $Zn_{0.8}Mn_{0.1}Co_{0.1}O$ and $Zn_{0.9}Mn_{0.05}Co_{0.05}O$ samples, for the same calcination temperatures are shown in Fig. 2(a) and (b), respectively. For calcination temperature of 300 °C, XRD patterns reveal that the samples are in single phase with ZnO wurtzite structure with the absence of any metallic

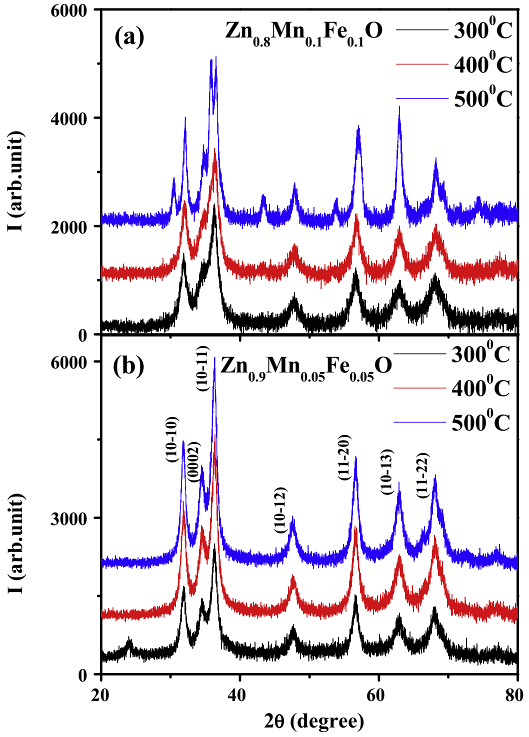

Fig. 1. (a) XRD patterns of $Zn_{0.8}Mn_{0.1}Fe_{0.1}O$, and (b) $Zn_{0.9}\ Mn_{0.05}Fe_{0.05}O$ nanoparticles calcined at 300, 400 and 500 °C.

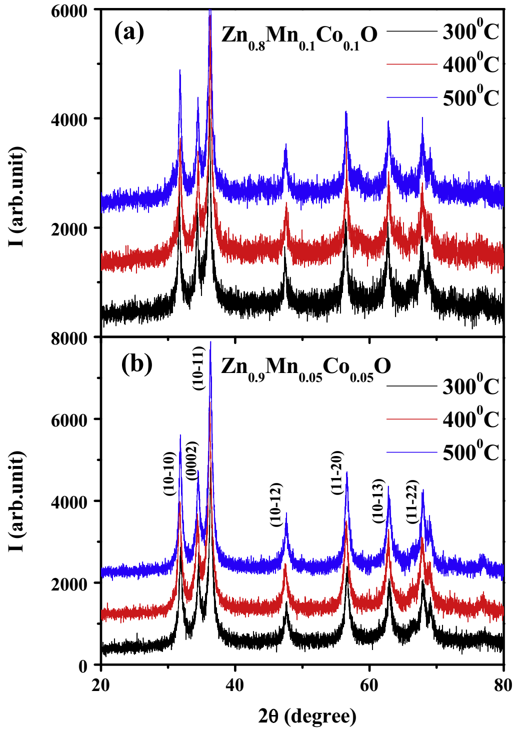

Fig. 2. (a) XRD patterns of $Zn_{0.8}Mn_{0.1}Co_{0.1}O$, and (b) $Zn_{0.9}\ Mn_{0.05}Co_{0.05}O$ nanoparticles calcined at 300, 400 and 500 °C.

and oxide peaks of the related doping elements, within the experimental limitations. From high-resolution (HR) XRD also, we could not detect any peak corresponding to any precipitate of doping element. At next higher calcination temperature, the secondary phase is found to just grow and enhance with further increasing calcination temperatures. Here our motivation is to study the physical properties of the single phase sample only. Thus, we have confined our study on sample, calcined at 300 °C. Detailed XRD studies on $Zn_{1-x}Mn_xO$ sample have been discussed in Ref. [17]. Low magnification bright field TEM micrographs are shown in Fig. 3, indicate nanometric particle size distribution in the range of ~2–40 nm. FE-SEM micrographs and EDAX spectra, shown in Figs. 4 and 5, respectively, correspond to absence of any phase segregation and good chemical homogeneity of these nanoparticles. Thermal analyses of those samples have been carried out using TG-DTA, as shown in Fig. 6(a) –(c). TG data show weight loss in three steps at 253, 411 and 490 °C for $Zn_{0.9}Mn_{0.1}O$ nanoparticles, at 274, 327 and 428 °C for $Zn_{0.8}Mn_{0.1}Fe_{0.1}O$ nanoparticles and at 244, 386 and 458 °C for $Zn_{0.8}Mn_{0.1}Co_{0.1}O$ nanoparticles. All the observed peaks in TG and DTA curves of the samples (Fig. 6) correspond to the exothermic peaks in the measured temperature range. In case of $Zn_{0.9}Mn_{0.1}O$ nanoparticles, the observed exothermic peaks at 253 and 411 °C are due to dehydration and that at 490 °C is due to decomposition of nanometric sample. In case of $Zn_{0.8}Mn_{0.1}Fe_{0.1}O$ nanoparticles, the exothermic peaks at 274 and 327 °C are due to dehydration and 428 °C is due to decomposition of nanometric sample. In case of $Zn_{0.8}Mn_{0.1}Co_{0.1}O$ nanoparticles the two exothermic peaks at 244 and 386 °C are due to dehydration and the peak at 458 °C is due to decomposition of nanometric sample.

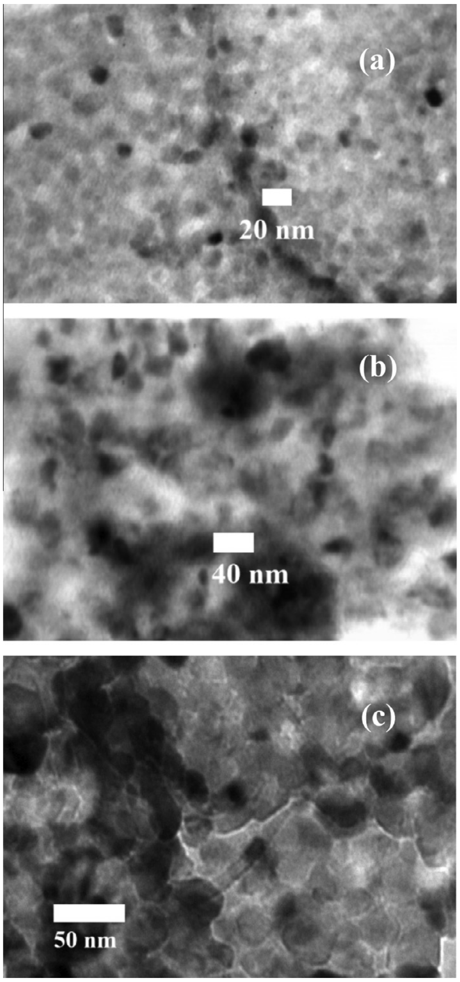

Fig. 3. Low magnification bright field TEM images for (a) $Zn_{0.9}Mn_{0.1}O$, (b) $Zn_{0.8}Mn_{0.1}Fe_{0.1}O$ and (c) $Zn_{0.8}Mn_{0.1}Co_{0.1}O$ nanoparticles.

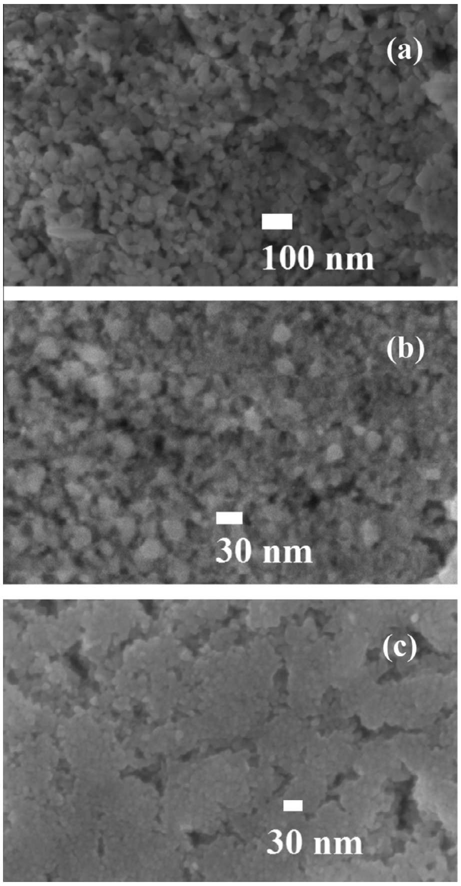

Fig. 4. FE-SEM images for (a) $Zn_{0.9}Mn_{0.1}O$, (b) $Zn_{0.8}Mn_{0.1}Fe_{0.1}O$ and (c) $Zn_{0.8}Mn_{0.1}Co_{0.1}O$ nanoparticles.

3.2. Dielectric studies

ε as a function of frequency (f) for $Zn_{1-x}Mn_xO$, $Zn_{1-x}Mn_{x/2}Fe_{x/2}O$ and $Zn_{1-x}Mn_{x/2}Co_{x/2}O$ nanoparticles at different x are shown in Fig. 7(a) –(c), respectively. ε shows usual exponential decrease with f revealing Maxwell–Wagner dispersion interfacial polarization phenomenon [24], which is in agreement with Koop's theory [25]. Insets in Fig. 7(a) –(c) shows ε as a function of x of the corresponding samples at low frequency (f = 115 Hz). A maxima in ε is found to appear at $x = 0.1$ for both $Zn_{1-x}Mn_xO$ and $Zn_{1-x}Mn_{x/2}Fe_{x/2}O$ nanoparticles, followed by decrease in ε with further increase in x. Quite differently, ε is found to increase continuously with increase in Co content in ZnMnO matrix. Simultaneously, we have carried out dielectric loss ($\tan\delta$) measurement for all those corresponding samples, as shown in Fig. 8(a)–(c), respectively. $\tan\delta$ is found to exhibit usual exponential decrease with increase in f for $x = 0$ i.e., for ZnO nanoparticles. The values of $\tan\delta$ show slightly higher value (<4.6) at low frequency region for $Zn_{1-x}Mn_xO$, $Zn_{1-x}Mn_{x/2}Fe_{x/2}O$ and $Zn_{1-x}Mn_{x/2}Co_{x/2}O$ nanoparticles compared to ZnO nanoparticles. These entire series of TM doped ZnMnO nanoparticles show maxima in $\tan\delta$ in the measured frequency range (Fig. 8).

Enhancement in ε from that of undoped ZnO is maximum for $Zn_{1-x}Mn_{x/2}Fe_{x/2}O$ sample compared to that of $Zn_{1-x}Mn_xO$ and $Zn_{1-x}Mn_{x/2}Co_{x/2}O$ sample (for $x = 0.1$ doping). Such enhancement in ε is found to be ~1500 times for $Zn_{0.9}Mn_{0.05}Fe_{0.05}O$ and ~2 times

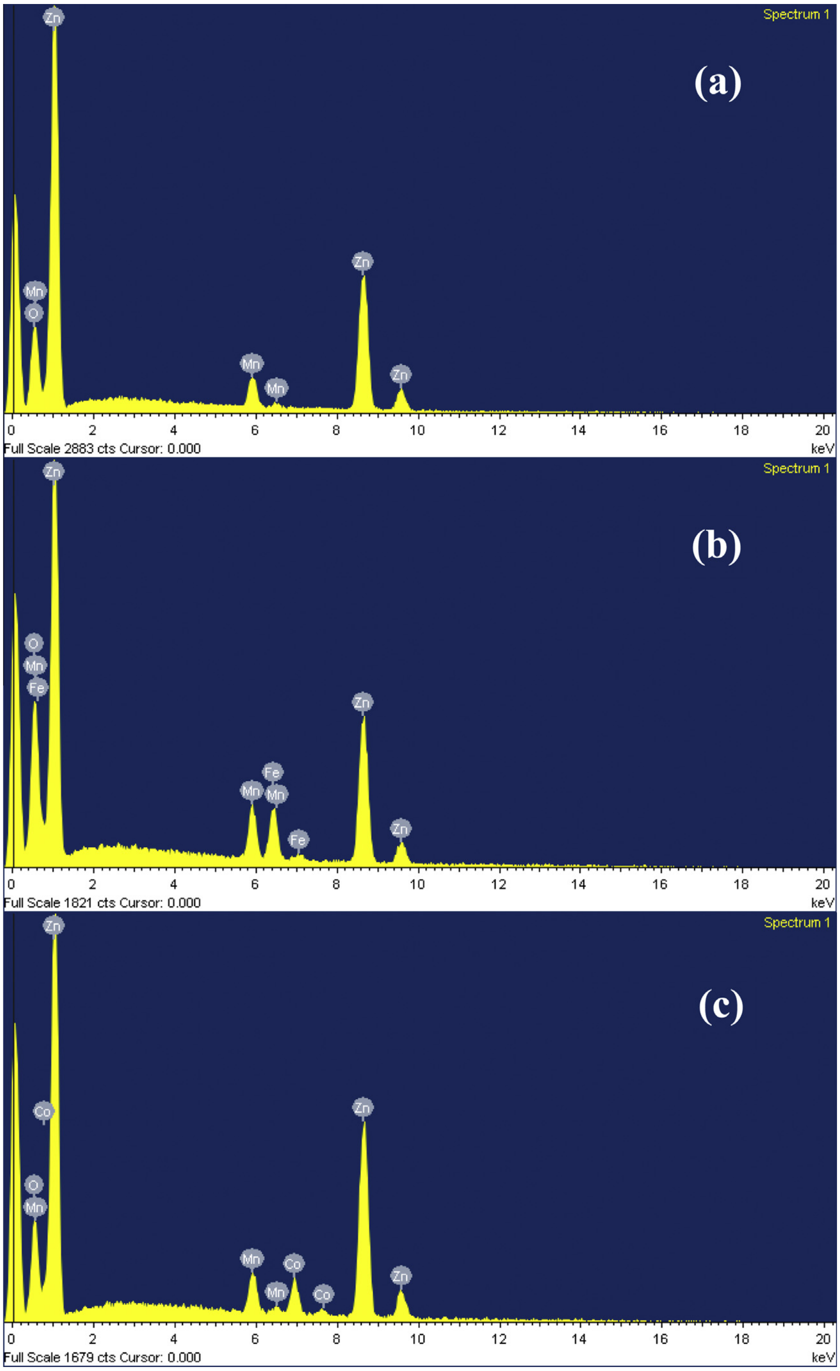

Fig. 5. EDAX spectra for (a) $Zn_{0.9}Mn_{0.1}O$, (b) $Zn_{0.8}Mn_{0.1}Fe_{0.1}O$ and (c) $Zn_{0.8}Mn_{0.1}Co_{0.1}O$ nanoparticles.

for $Zn_{0.9}Mn_{0.05}Co_{0.05}O$ nanoparticles from that of $Zn_{0.9}Mn_{0.1}O$ nanoparticles at room temperature. This is clearly shown in bar diagram in Fig. 9(a). Similar bar diagram for $x = 0.2$ doped samples is shown in Fig. 9(b). From this bar diagram, an enhancement of ε is observed by ~20 times for $Zn_{0.8}Mn_{0.1}Fe_{0.1}O$ and ~18 times for $Zn_{0.8}Mn_{0.1}Co_{0.1}O$ nanoparticles, compared to that of $Zn_{0.8}Mn_{0.2}O$ nanoparticles at room temperature. Thus, from this bar analysis one can choose the doping element, along with dopant concentration to get the desired higher value of ε in TM doped ZnMnO nanoparticles at room temperature.

In our sample, doping of Fe and Co element in ZnMnO matrix determines the extent of enhancement in ε. In case of Fe doping in ZnMnO matrix, a huge enhancement in ε is observed as compared to Co doping. When TM (Fe, Co) is doped in the substitutional Mn/Zn site then it has the possibility to be in Fe^{2+}/Co^{2+} ionic sate. However, it is quite possible that a large number of uncoupled Fe^{3+}/Co^{3+} ions are present in the sample in order to maintain charge imbalance, created by Zn vacancies. This happens by changing the ionic state from $Fe^{2+} \leftrightarrow Fe^{3+}/Co^{2+} \leftrightarrow Co^{3+}$ in ZnMnO matrix. This changing of ionic state of the TM ions in the system leads to effective doping of higher oxidation state of TM ions in ZnMnO matrix. Infact, existence of such vacancy sites and consequently the charge mixing has been found in this kind of nanocrystalline transition metal doped ZnO DMS samples

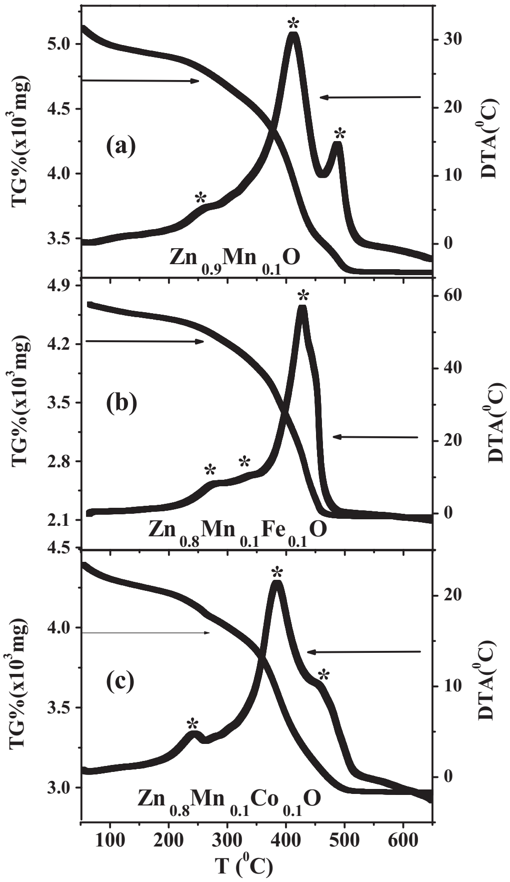

Fig. 6. TG-DTA for (a) $Zn_{0.9}Mn_{0.1}O$, (b) $Zn_{0.8}Mn_{0.1}Fe_{0.1}O$ and (c) $Zn_{0.8}Mn_{0.1}Co_{0.1}O$ nanoparticles.

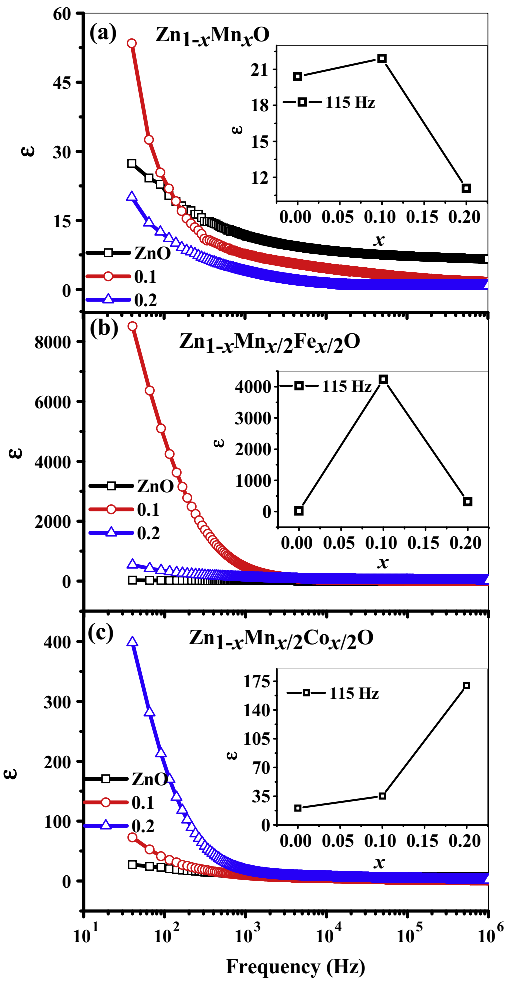

Fig. 7. ε as a function of frequency with varying doping level x for (a) $Zn_{1-x}Mn_xO$, (b) $Zn_{1-x}Mn_{x/2}Fe_{x/2}O$ and (c) $Zn_{1-x}Mn_{x/2}Co_{x/2}O$. Inset shows ε as a function of doping level x at $f = 115$ Hz for corresponding samples.

[26,27]. In this context, the formation of space charge polarization is highly possible that in turn results in this observed enhancement of ε up to a certain x, as discussed in our previous paper [20]. Moreover, we are working on nanoparticles samples, as is evident from TEM micrographs. Thus the surface to volume ratio is expected to be quite large and the surface related physical properties are supposed to be appreciably pronounced in the system. Moreover, our samples are heavily TMs doped samples. Thus the number of TM ions residing at the grain surface is expected to be quite larger than its bulk region. It can be easily understood that TM ions residing at the enhanced grain surface are expected to be in higher and stable oxidation state [17,18]. For Fe and Co ions, the stable and higher oxidation state is Fe^{3+} and Co^{3+} in ZnMnO matrix. So, there is quite possibility of the presence of large number of uncompensated TM ions at the enhanced grain surface of the nanoparticles. Furthermore, *d*-orbital element with half-filled subshell is the most stable. The ground state configuration for Fe^{3+} is [Ar] $3d^5$ and for Co^{3+} is [Ar] $3d^6$, indicating that Fe^{3+} ion is more stable than Co^{3+}. As a result, we may expect a more abundance of Fe^{3+} ion as compared to Co^{3+} ions on the grain boundary in our samples. This, in turn causes enhanced dielectric polarization in ZnMnFeO than ZnMnCoO sample. Consequently, enhancement in ε is found to be much larger in $Zn_{0.9}Mn_{0.05}Fe_{0.05}O$ (∼1500 times) and in $Zn_{0.8}Mn_{0.1}Co_{0.1}O$ (∼10 times) nanoparticles from that of $Zn_{0.9}Mn_{0.1}O$ nanoparticle at room temperature. Similarly, the observed higher value of ε of $Zn_{0.9}Mn_{0.1}O$ sample compared to ZnO, can be explained considering the Zn vacancy sites that in turn induces charge imbalance in the system.

3.3. Optical property

To investigate the semiconducting band gap (E_g) of those samples, we have recorded the absorbance spectra at room temperature using a UV – visible spectrophotometer. Absorbance spectra of the $Zn_{0.9}Mn_{0.1}O$ and $Zn_{0.9}Mn_{0.05}Fe_{0.05}O$ samples, as shown in Fig. 8(a) and (b), respectively, do not show very sharp absorption edge. This behavior may be due to broad nanometric particle size distribution of those samples. In such case, E_g of those samples can be estimated from the maximum in the first derivative curve of each absorbance spectrum [28]. Insets in Fig. 10(a) and (b) shows the first derivative curve of absorbance spectra for $Zn_{0.9}Mn_{0.1}O$ and $Zn_{0.9}Mn_{0.05}Fe_{0.05}O$ samples, respectively. From the Gaussian fit of these first derivative curves, the points of inflection have been estimated. This point of inflection can be considered to represent the absorption edge of absorbance spectra, from which the band gap energy is estimated to be $E_g = 3.29$ eV for $Zn_{0.9}Mn_{0.1}O$ and $Zn_{0.9}Mn_{0.05}Fe_{0.05}O$ samples. This value of E_g is equivalent to the estimated band gap energy (not shown here) for other samples, discussed here.

4. Conclusions

In conclusions, $Zn_{1-x}Mn_xO$, $Zn_{1-x}Mn_{x/2}Fe_{x/2}O$ and $Zn_{1-x}Mn_{x/2}Co_{x/2}O$ nanoparticles were prepared through low temperature

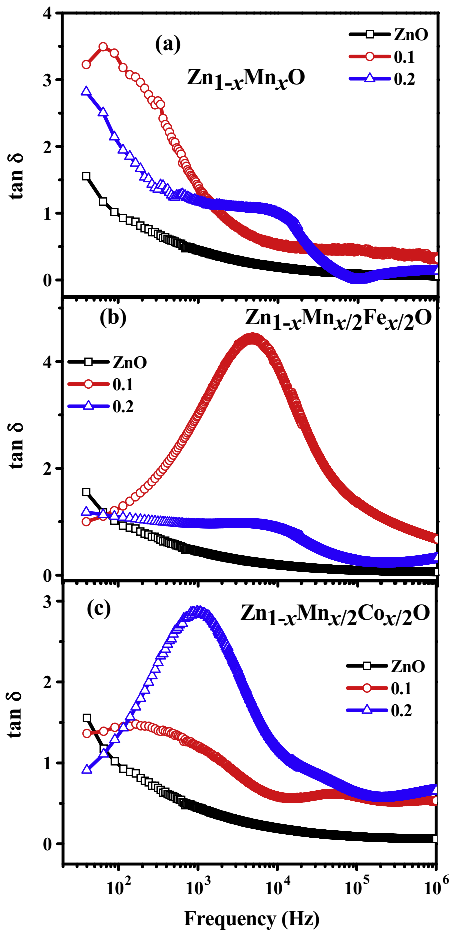

Fig. 8. tan δ as a function of frequency for (a) $Zn_{1-x}Mn_xO$, (b) $Zn_{1-x}Mn_{x/2}Fe_{x/2}O$ and (c) $Zn_{1-x}Mn_{x/2}Co_{x/2}O$ at 300 K with varying x.

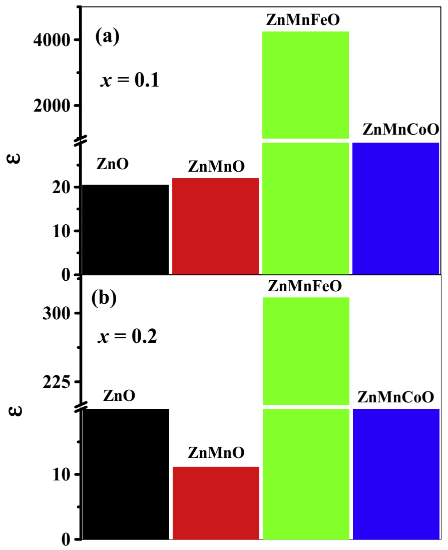

Fig. 9. Different value of ε for different doping element with doping level (a) $x = 0.1$, (b) $x = 0.2$ for $f = 115$ Hz at 300 K.

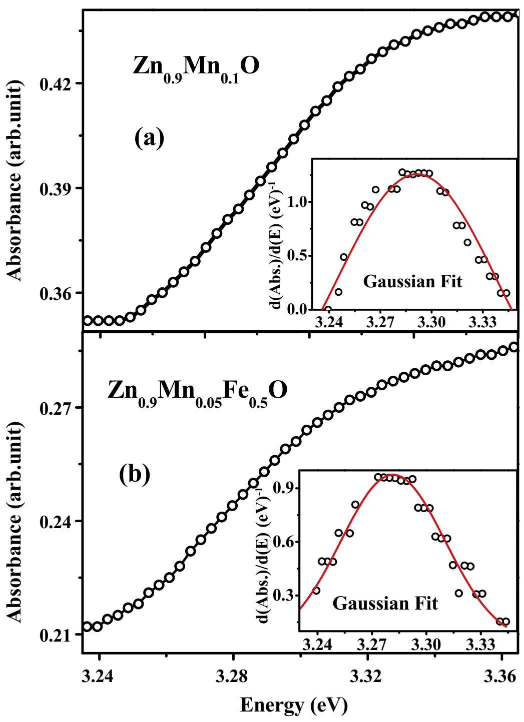

Fig. 10. Optical absorbance spectra for (a) $Zn_{0.9}Mn_{0.1}O$ and (b) $Zn_{0.9}Mn_{0.05}Fe_{0.05}O$ nanoparticles, measured at 300 K. Insets show the derivative plot of absorbance spectra fitted with the Gaussian function, from which the semiconducting band gap is estimated to be $E_g = 3.29$ eV.

chemical pyrophoric reaction process. Structural analyses reveal the formation of single phase nanoparticles with an average particle size of ~2–40 nm. ε as function of f and doping concentration, x has been studied at room temperature. At low frequency range, ($f \sim 115$ Hz), enhancement in ε is found to be ~1500 times for $Zn_{0.9}Mn_{0.05}Fe_{0.05}O$ and ~10 times for $Zn_{0.8}Mn_{0.1}Co_{0.1}O$ nanoparticles from that of $Zn_{0.9}Mn_{0.1}O$ nanoparticles. Such variation in enhancement in ε can be explained on the basis of dielectric polarization, induced by the presence of different abundance of Fe^{3+} and Co^{3+} ions in ZnMnFeO and ZnMnCoO nanoparticles, respectively. From our observation, one can identify the right choice of TM and its doping level, x to achieve a desired enhancement of ε, commensurate with the corresponding dielectric loss, for TM doped ZnO nanoparticles. Thus $Zn_{0.9}Mn_{0.05}Fe_{0.05}O$ sample seems to be a promising candidate for high k-dielectric application. The semiconducting band gap of those nanoparticles has been estimated using recorded absorbance spectra at room temperature.

Acknowledgement

One of the authors S.K. Mandal acknowledges the DST Project (No. SR/FTP/PS-019/2012), India for financial support. We acknowledge Dr. A. Nath (NIT Agartala) and IIT Kharagpur, India for providing us some experimental facilities.

References

[1] F. Pan, C. Song, X.J. Liu, Y.C. Yang, F. Zeng, Mater. Sci. Eng.: R: Rep. 62 (2008) 1–35.
[2] R. Khan, A. Kaushik, P.R. Solanki, A.A. Ansari, M.K. Pandey, B.D. Malhotra, Anal. Chim. Acta 616 (2008) 207–213.
[3] A. Yadav, V. Prasad, A.A. Kathe, S. Raj, D. Yadav, C. Sundaramoorthy, N. Vigneshwaran, Bull. Mater. Sci. 29 (2006) 641–645.
[4] G. Shan, X. Kong, X. Wang, Y. Liu, Surf. Sci. 582 (2005) 61–68.
[5] A.B. Djurišić, A.M.C. Ng, X.Y. Chen, Prog. Quant. Elec. 34 (2010) 191–259.
[6] H. Zulkefle, L.N. Ismail, R.A. Bakar, M.H. Mamat, M. Rusop, Int. J. Appl. Phys. Math. 2 (2012) 38–43.
[7] N.T. Salim, K.C. Aw, W. Gao, B.E. Wright, Thin Solid Films 518 (2009) 362–365.

[8] M.S. Samuel, J. Koshy, A. Chandran, K.C. George, Curr. Appl. Phys. 11 (2011) 1094–1099.
[9] K. Omar, Modern Appl. Sci. 3 (2009) 110–116.
[10] C.K. Ghosh, S. Malkhandi, M.K. Mitra, K.K. Chattopadhyay, J. Phys. D Appl. Phys. 41 (2008) 1–9.
[11] S.J. Pearton, D.P. Norton, K. Ip, Y.W. Heo, T. Steiner, Super Lattices Microstruct. 34 (2003) 3–32.
[12] Y. Yang, W. Guo, X. Wang, Z. Wang, J. Qi, Y. Zhang, Nano Lett. 12 (2012) 1919–1922.
[13] S.S. Batsanov, K.B. Poyarkov, S.M. Gavrilkin, Dokl. Phys. 54 (2009) 407–409.
[14] A.S. Lanje, S.J. Sharma, R.S. Ningthoujam, J.-S. Ahn, R.B. Pode, Adv. Pow. Tech. 24 (2013) 331–335.
[15] G. Murugadoss, J. Mater. Sci. Technol. 28 (2012) 587–593.
[16] S. Senthilkumar, K. Rajendran, S. Banerjee, T.K. Chini, V. Sengodan, Mater. Sci. Semicond. Process. 11 (2008) 6–12.
[17] S.K. Mandal, A.K. Das, T.K. Nath, D. Karmakar, B. Satpati, J. Appl. Phys. 100 (2006) 104315-1–104315-8.
[18] D. Karmakar, S.K. Mandal, R.M. Kadam, P.L. Paulose, A.K. Rajarajan, T.K. Nath, A.K. Das, I. Dasgupta, G.P. Das, Phys. Rev. B 75 (2007) 144404-1–144404-14.
[19] D. Karmakar, T.V. Chandrasekhar Rao, J.V. Yakhmi, A. Yaresko, V.N. Antonov, R.M. Kadam, S.K. Mandal, R. Adhikari, A.K. Das, T.K. Nath, N. Ganguli, I. Dasgupta, G.P. Das, Phys. Rev. B 81 (2010) 184421-1–184421-13.
[20] S. Singh, P. Dey, J.N. Roy, S.K. Mandal, Appl. Phys. Lett. 105 (2014) 092903-1–092903-4.
[21] S.K. Mandal, T.K. Nath, A.K. Das, D. Karmakar, J. Appl. Phys. 101 (2007) 063913-1–063913-6.
[22] S.K. Mandal, T.K. Nath, A. Das, J. Appl. Phys. 101 (2007) 123920-1–123920-7.
[23] S.K. Mandal, A.K. Das, T.K. Nath, D. Karmakar, Appl. Phys. Lett. 89 (2006) 144105-1–144105-3.
[24] K.W. Wagner, Amer. Phis. 40 (1973) 817.
[25] C.G. Koops, Phys. Rev. 83 (1951) 121.
[26] H.S. Hsu, J.C.A. Huang, Y.H. Huang, Y.F. Liao, M.Z. Lin, C.H. Lee, J.F. Lee, S.F. Chen, L.Y. Lai, C.P. Liu, Appl. Phys. Lett. 88 (2006) 242507-1–242507-3.
[27] H.S. Hsu, J.C.A. Huang, S.F. Chen, C.P. Liu, Appl. Phys. Lett. 90 (2007) 102506-1–102506-3.
[28] S. Sapra, R. Viswanatha, J. Nanda, D.D. Sarma, in: D. Bahadur, S. Vitta, O. Prakash (Eds.), Inorganic Materials: Recent Advances, first ed., Narosa Publishing House, New Delhi, 2004, p. 452.